Biol Trace Elem Res (2007) 118:233–243
DOI 10.1007/s12011-007-0028-6

Transport of Intranasally Instilled Fine Fe_2O_3 Particles into the Brain: Micro-distribution, Chemical States, and Histopathological Observation

Bing Wang · Wei Y. Feng · Meng Wang · Jun W. Shi · Fang Zhang · Hong Ouyang · Yu L. Zhao · Zhi F. Chai · Yu Y. Huang · Ya N. Xie · Hai F. Wang · Jing Wang

Received: 13 July 2006 / Revised: 17 January 2007 / Accepted: 24 February 2007 /
Published online: 26 May 2007

Abstract It has been demonstrated that inhaled fine (d<2.5 μm) and ultrafine (d<100 nm) particles produce more severe toxicity than coarse particles. Some recent data support the concept that the central nervous system (CNS) may be a target for the inhaled fine particulates. This work describes initial observation of the transport of intranasally instilled fine ferric oxide (Fe_2O_3) particles in animal brain. The iron micro-distribution and chemical state in the mice olfactory bulb and brain stem on day 14 after intranasal instillation of fine Fe_2O_3 particle (280±80 nm) suspension at a single dose of 40 mg/kg body weight were analyzed by synchrotron radiation x-ray fluorescence and x-ray absorption near-edge structure (XANES). The micro-distribution map of iron in the olfactory bulb and brain stem shows an obvious increase of Fe contents in the olfactory nerve and the trigeminus of brain stem, suggesting that Fe_2O_3 particles were possibly transported via uptake by sensory nerve endings of the olfactory nerve and trigeminus. The XANES results indicate that the ratios of Fe (III)/Fe (II) were increased in the olfactory bulb and brain stem. The further histopathological observation showed that the neuron fatty degeneration occurred in the CA3 area of hippocampus. Such results imply an adverse impact of inhalation of fine Fe_2O_3 particles on CNS.

B. Wang · W. Y. Feng (✉) · M. Wang · J. W. Shi · H. Ouyang · Y. L. Zhao · Z. F. Chai
Laboratory for Bio-Environmental Effects of Nanomaterials and Nanosafety and Key Laboratory of Nuclear Analytical Techniques, Institute of High Energy Physics, Chinese Academy of Sciences, Beijing, China
e-mail: fengwy@mail.ihep.ac.cn

B. Wang · M. Wang · J. W. Shi · F. Zhang
Graduate School of Chinese Academy of Sciences, Beijing, China

Z. F. Chai
Institute of Nuclear Technology, Shenzhen University, Shenzhen, China

Y. Y. Huang · Y. N. Xie
Beijing Synchrotron Radiation Laboratory, Institute of High Energy Physics, Chinese Academy of Sciences, Beijing, China

H. F. Wang · J. Wang
College of Chemistry and Molecular Engineering, Peking University, Beijing, China

Keywords Fine ferric oxide particle · Intranasal instillation · Olfactory transportation · Brain · Micro-distribution · Chemical state · Pathological observation

Introduction

Epidemiological studies conducted in Europe and the United States have demonstrated that inhaled fine (d<2.5 μm) particles are strongly associated with respiratory and cardiovascular system diseases [1–3]. Many toxicological studies over the last 10 years indicate that particles in the ultrafine size range (d<100 nm) are likely responsible for most of the adverse health effects [4, 5]. Recently, interest in the non-pulmonary targets of inhaled particles has been increasing, as some studies have demonstrated that inhaled fine and ultrafine particles could quickly left the lung and deposit in extra-pulmonary tissues [6, 7]. Some recent data support the concept that the brain might be another potential target organ for inhaled fine and ultrafine particles [8, 9]. The engineered nanoparticles are of the same size as aerosol ultrafine particles. With the development of the nano-industry, people are at significantly elevated health risks of acute fine and ultrafine particle exposure. The investigation of the fate of the inhaled engineered fine and ultrafine particles in extra-pulmonary site is important for estimation their effects in the target organs.

Depending on the size of fine and ultrafine particle, inhaled nanoparticles are more efficient to deposit in the nasal mucous [9]. The primary olfactory neurons in the olfactory mucosa provide a direct contact with the external environment in the nasal cavity, thus, present a route for exogenous substances to enter the brain [10]. Many studies have shown that the olfactory tract is an important access for metal ions and inhaled foreign particles entering the brain bypass the blood-brain barrier [8–12]. In this study, we hypothesized that fine particle uptake in the olfactory epithelium could transport along the olfactory neurons and enter the brain. We selected fine ferric oxide (Fe_2O_3) particle representing as a kind of mildly soluble material to observe its possible transportation into the brain via olfactory pathway after intranasal instillation.

Iron in the brain has been extensively studied because of its ability to produce neurotoxicity after high dose occupational exposure [13, 14]. Abnormal accumulation of iron in the brain has been implicated in a variety of neurodegenerative diseases, including Hallervorden-Spatz, Parkinson's disease (PD), and Alzheimer's disease (AD) [14, 15]. Some evidence indicates that iron accumulation in brain regions is an initial event that causes neuronal death or is a consequence of some disease processes [16]. Iron as a redox-active transition metal can play a pivotal role in the formation of hydroxyl radicals through the Fenton reaction in vivo. Oxidative stress resulted from increased iron levels in brain and possibly from defects in antioxidant defense mechanisms is believed to associate with neuronal death in those neurodegenerative disorders [14, 15]. Therefore, we are extremely concerned about whether the mildly soluble fine or ultrafine iron particles could transport into the brain like other metals via olfactory pathway during high level inhalation. It has been known that the process of olfactory transportation depends on several factors including particle solubility, particle size, the site of deposition, and so forth [16]. Rao et al. [17] found that $FeSO_4$ aerosol was not readily transported to the brain via the olfactory tract. However, it has not been known yet whether the iron particles could transport into brain when particles deposit in the nasal mucous.

In our earlier pilot study, the significant increase of iron contents in the mouse olfactory bulb (OB) and deep brain regions had been observed after intranasal instillation of fine Fe_2O_3 particles, which led us to hypothesize that the routes for translocation of fine or

ultrafine Fe_2O_3 particle to the central nervous system (CNS) via the olfactory tract existed. Therefore, a more detailed study was conducted by synchrotron radiation x-ray fluorescence (SRXRF) and x-ray absorption near-edge structure (XANES) on iron micro-distribution and chemical state in the OB and brain stem after intranasal instillation of fine Fe_2O_3 particle to the mice.

Materials and Methods

Preparation of Fine Fe_2O_3 Particle Suspension

The fine Fe_2O_3 particle was purchased from Shi-Jia Wei-Er Co. Ltd., Chengdu, China. The mean size of the Fe_2O_3 particle was measured as 280±80 nm by transmission electron microscopy (TEM; see Fig. 1). The Fe_2O_3 particle was suspended in 1% sodium carboxy methyl cellulose, stirred on vortex agitator, and dispersed by ultrasonic vibration for at least 15 min before use.

Animal Experiment

Healthy CD-ICR male mice of 4 weeks old and 20- to 22-g weight were supplied by the Department of Laboratory Animal Science, Peking University Health Center. The mice were maintained on the commercial pellet diet and deionized water ad libitum and kept in plastic cages in a 20±2°C, 50–70% relative humidity room with a 12-h light/dark cycle. The exposed group mice were instilled intranasally in the right nasal cavity with 40-mg fine Fe_2O_3 particle per kilogram body weight. The control mice were given by the same volume of 1% sodium carboxy methyl cellulose solution instead.

SRXRF and XANES Study

On day 14 after intranasal exposure, the mice were killed, and the brains were quickly removed. The OB and brain stem were frozen; coronally cut into 80-μm slice, then fixed onto a polycarbonate film, and dried in a clean box. Because of the limitation of experimental time, three exposed and three control samples were studied.

The SRXRF experiment was performed at the Beijing Synchrotron Radiation Facility (BSRF) 3W1A X-ray fluorescence station in the Institute of High Energy Physics, Chinese

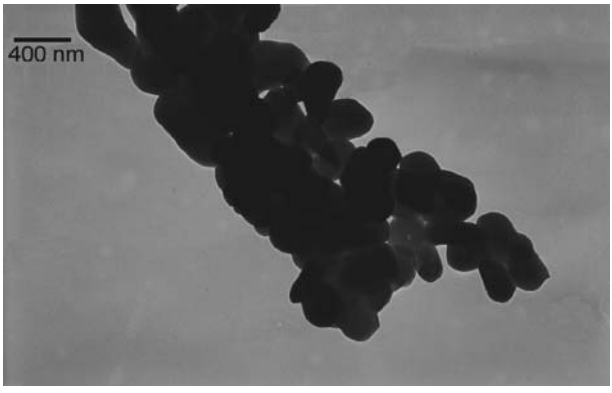

Fig. 1 TEM image of ferric oxide particle

Academy of Sciences. The beam line from the storage ring (2.5 GeV, maximum current 120 mA) can provide multi-chromatic x-rays of energy range from 3.5 to 35 keV. Considering the limit of detection, the cross-section of the beam irradiating on the sample was adjusted to about 60×80 μm by a Pb collimator with two cross-slices. The iron micro-distributions in the right OB and the whole brain stem were studied. The sample platform was moved by a two-dimensional stepping motor. The Fe distribution in the OB was continuously scanned at a step of 150 μm for the X direction and 200 μm for the Y direction. For the brain stem sample, the scan was performed by 300 μm step-size along the X direction and 200 μm along the Y direction. About 200 points were measured for each OB slice and 210 points for brain stem one. Each spot was irradiated for about 60 s. The x-ray spectra were analyzed by the AXIL program, and all x-ray spectra and their Compton scattering intensity were normalized to the collecting time and the counting of the ionization chamber. The relative content of Fe was obtained by the ratio of net x-ray peak area (with subtracting the contribution of the polycarbonate film) to the relative Compton scattering intensity. Then, the micro-distribution map of Fe in the brain region can be obtained.

The XANES spectra were collected at the beam line 1W1B of BSRF. The synchrotron radiation was monochromatized by a Si (111) double crystal monochromator. Harmonic rejection was achieved by detuning the second crystal of the monochromator. Energy resolution was estimated to be about 0.3 eV by the copper foil three-dimensional near-edge feature. The beam size on the sample was 900×300 μm^2. Energy calibration was monitored using an iron foil and was set as 7.112 keV. Iron K-edge XANES spectra were recorded from 200 eV below to 200 eV above the iron K-edge threshold energy (7.112 keV). The data of FeO and Fe_2O_3 chemical standards were collected at transmission mode using ion chamber with N_2/Ar filled gas. The fluorescence signal of brain samples was detected by a Lytle fluorescence ionization chamber. The absorption coefficients were calculated from the incident (I_0) and transmission intensity (I) or fluorescence intensity (I_f), and the data normalization was carried out by WINXAS 97.

Histopathological Observation

After the mice were killed, the brains were quickly removed and fixed in 10% formalin, and then embedded into paraffin, sectioned for 5-μm thick, and finally mounted on the glass microscope slides using standard histopathological techniques. The sections were stained with hematoxylin–eosin and examined by optical microscopy.

Results

Fe Micro-distribution in the OB and Brain Stem by SRXRF

In this study, the coronal section of the OB was present coexistently with the plane of OB and olfactory peduncle (OP). Olfactory bulb includes the main olfactory bulb (MOB) and accessory OB as well. The anatomic map of the MOB could be distinguished as six layers from outside to inside: olfactory nerve layer (ON), glomerular layer (Gl), external plexiform layer, mitral cell layer, internal plexiform layer, and granule cell layer of olfactory bulb [18]. Olfactory peduncle, the ventrolateral portion below the OB, contains lateral olfactory tract (lo), anterior olfactory nucleus (AO), and intermediate olfactory tract. Figure 2 shows a typical micro-distribution map of Fe in the right OB of the control and exposed mice. The

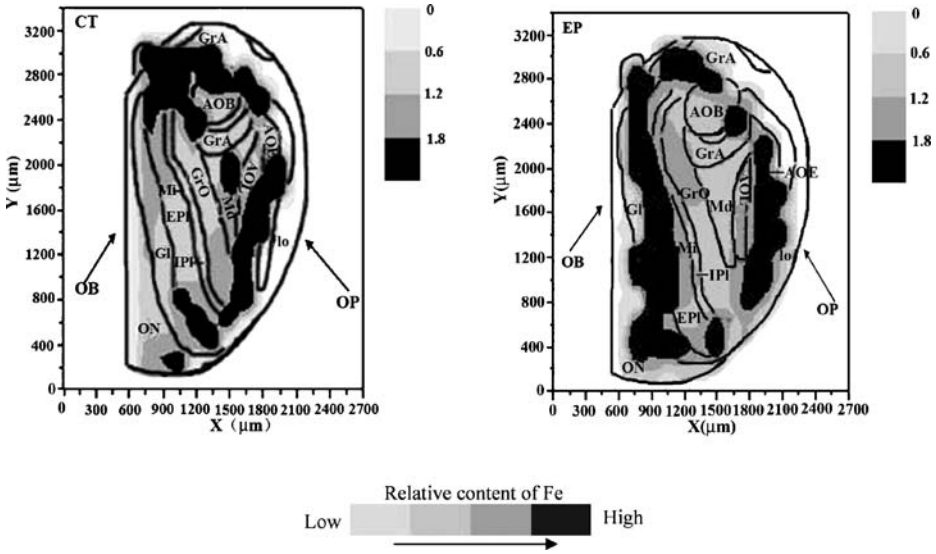

Fig. 2 Fe distribution in the OB section. CT = Control group (n=3); EP = exposed group (n=3). OB = olfactory bulb; OP = olfactory peduncle; ON = olfactory nerve; Gl = glomerular layer; Epl = external plexiform layer, Mi = mitral cell layer; Ipl = internal plexiform layer; GrO = granule cell layer of olfactory bulb; Md = medullary layer; GrA = granule cell layer of accessory olfactory bulb; AOB = accessory olfactory bulb; AOE = anterior olfactory nucleus external part; AOL = anterior olfactory nucleus, lateral part; lo = lateral tract

data show that the average content of Fe in the exposed mice was about 31% higher than in the control mice. Compared with the controls, the Fe contents in the exposed mice significantly increased in the ON, Gl of OB, and anterior olfactory nucleus external part (AOE), lo of OP layers (Fig. 2).

Gray matter areas in the brain stem include a variety of nuclei related with somatic and visceral motion, such as hypoglossal nucleus, trigeminal motor nucleus, facial nucleus, accessory nucleus ambiguus nucleus (Amb), and dorsal nucleus of vagus nerve [19]. Additionally, many sensory nuclei such as solitary tract nucleus, spinal trigeminal tract (sp5), vestibular nucleus, and so forth also exist in these areas [20]. The reticular formation in brain stem comprises of numerous nuclei responsible for motion and perception. The statistical results indicated that, in the brain stem sections, the Fe content increased by 21% in the exposed mice. The SRXRF micro-distribution map (Fig. 3) shows that the Fe content in the exposed mice elevated significantly in the reticular formation of the brain stem, such as paramedian reticular nucleus, gigantocellular reticular nucleus, dorsal paragigantocellular nucleus, lateral paragigantocellular nucleus, intermediate reticular nucleus, rostroventrolateral reticular nucleus, and parvicellular reticular nucleus. Additionally, in the spinal trigeminal regions of the brain stem, such as interpolar part (Sp5I), the Fe content distinctly increased as well. However, the Fe levels in the Amb, inferior olive, principal nucleus, and pyramidal tract decreased.

Fe K-edge XANES Analyses

Iron K-edge XANES analyses were applied to study Fe chemical state in brain samples. X-ray absorption near-edge structure-normalized spectra in brain specimen and standard

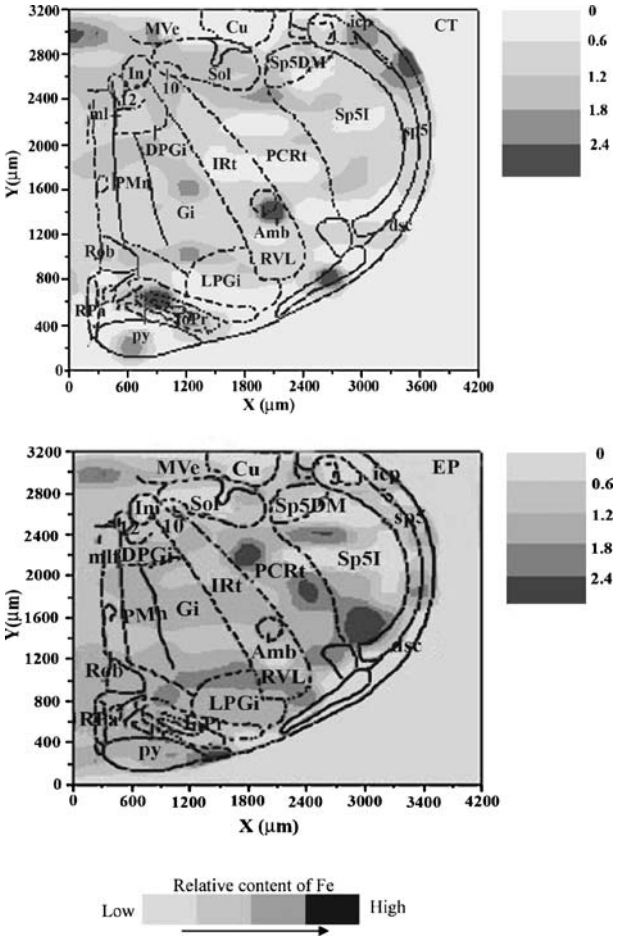

Fig. 3 Fe distribution in the brain stem section. CT = Control group (n=3); EP = exposed group (n=3). Mve = medial vestibular nucleus; Cu = cuneate nucleus; icp = inferior cerebellar peduncle; 12 = hypoglossal nucleus; 10 = dorsal motor nucleus of the vagus; In = intercalated nucleus; Sol = solitary tract nucleus; Sp5 = spinal trigeminal tract; Sp5DM = dorsomedial part of Sp5; Sp5I = interpolar part of Sp5; PCRt = parvicellular reticular nucleus; Irt = intermediate reticular nucleus; Gi = gigantocellular reticular nucleus; DPGi = dorsal paragigantocellular nucleus; LPGi = lateral paragigantocellular nucleus; Amb = ambiguus nucleus; mlf = medial longitudinal fasciculus; Rob = raphe obscurus nucleus; PMn = paramedian reticular nucleus; IOPr = inferior olive, principal nucleus; py = pyramidal tract; dsc = dorsal spinocerebellar tract; RPa = raphe pallidus nucleus

references (Fe_2O_3 and FeO powders) by edge step were diagrammed in Fig. 4. The edge step is defined as the difference between the pre-edge and post-edge fits extrapolated to the edge energy. The absorption edge (E_0) is defined by taking the maximum of the first derivative of the edge, and the edge shift is the chemical shift to FeO.

The data in Table 1 indicated that the E_0 values of iron in the OB of the control and exposed mice were 7.1245 and 7.1257 keV, respectively, and the E_0 of the exposed mice was the closest to the Fe_2O_3 standard compound (7.1265 keV). The E_0 values in the brain stem of the control and exposed mice were 7.1233 and 7.1240 keV, respectively. The E_0 in the OB and brain stem of the exposed mice were 1.2 and 0.7 eV higher than the corresponding control samples, respectively (see Fig. 4). Table 1 presents the calculated data of the iron edge shifts and the Fe (II)/Fe (III) ratios in the samples. The elevated Fe (III) levels in the exposed mice OB and brain stem were found in comparison with controls.

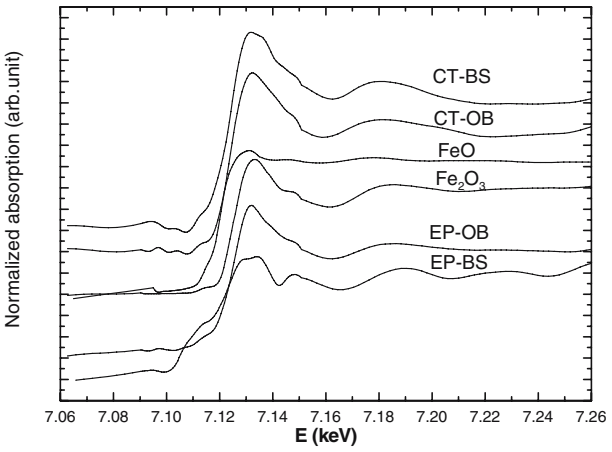

Fig. 4 Fe K-edge XANES spectra of sample and standard powders. CT-OB = Olfactory bulb of control group; CT-BS = brain stem of control group; EP-OB = olfactory bulb of exposed group; EP-BS = brain stem of exposed group. FeO = FeO powder; Fe_2O_3 = Fe_2O_3 powder

Histopathological Observation

The histopathological observation showed that there was a heavier fatty degeneration of neurocytes in the hippocampus CA3 area at the 14th day after intranasal instillation of fine Fe_2O_3 particles to the mice. All exposed mice presented the consistent pathological changes. Figure 5 shows typical pathological damage images for hippocampus of an exposed mouse. Besides the hippocampus, no pathological damage was found in other regions of the mice brain.

Discussions

In our early pilot study, we observed that significantly higher iron existed in the OB and could further transport into other brain regions, such as the brain stem after intranasal instillation. Therefore, to further understand the transport of inhaled fine Fe_2O_3 particle into the brain, the micro-distribution and chemical states of iron in the OB and brain stem were investigated.

Synchrotron radiation is an ideal x-ray source that provides continuum and high intensity photon for the investigation of trace metallic elements contained in biological specimens.

Table 1 Absorption Edge, Edge Shift, and Fe (II)/Fe (III) Ratio in the Brain Samples

	FeO	Fe_2O_3	Olfactory bulb		Brain stem	
			Control	Exposed	Control	Exposed
Absorption edge (keV)	7.1207	7.1265	7.1245	7.1257	7.1233	7.1240
Edge shift (eV)	0	5.8	3.8	5	2.6	3.3
Fe (II)/Fe (III) ratio[a]			0.53	0.16	1.23	0.76

$E_{Fe_2O_3}$ The absorption edge for Fe_2O_3 powder

E_s The absorption edge of Fe in olfactory bulb and brain stem slices

E_{FeO} The absorption edge for FeO powder

[a] The Fe (II)/Fe (III) ratio is calculated by the following equation: $\frac{\mathrm{Fe(II)}}{\mathrm{Fe(III)}} = \frac{E_{\mathrm{Fe_2O_3}} - E_s}{E_s - E_{\mathrm{FeO}}}$

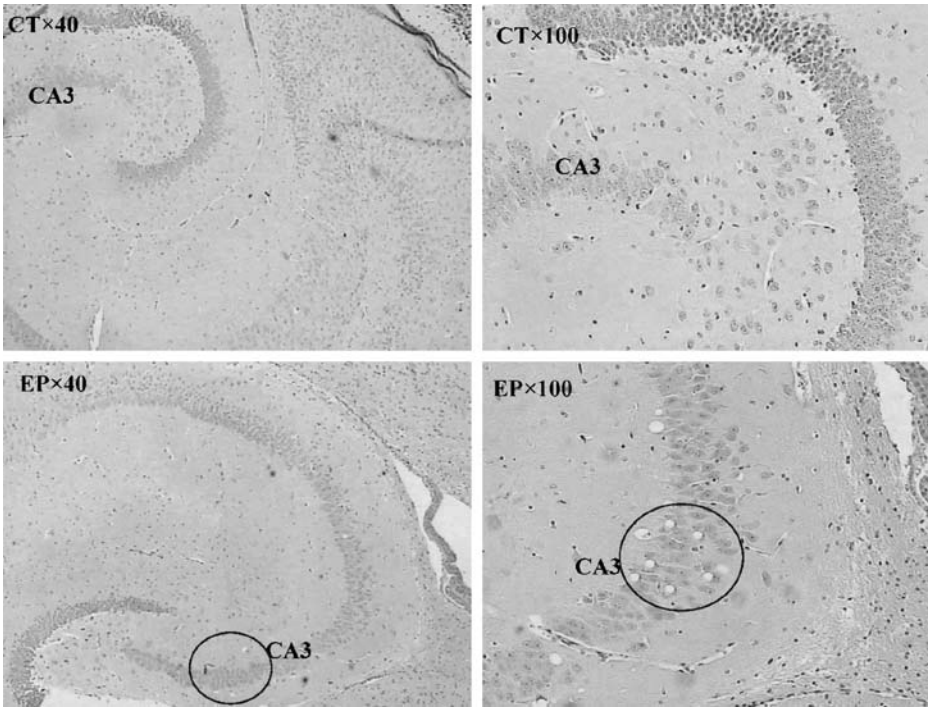

Fig. 5 Histopathological changes in hippocampus of the mice. CT×40 = Hippocampus in the control mice, magnification ×40; CT×100 = hippocampus in the control mice, magnification ×100. EP×40 = hippocampus in the exposed mice, magnification ×40; EP×100 = hippocampus in the exposed mice, magnification ×100. Circle areas show the fatty degeneration in CA3 neurons of hippocampus

SRXRF and XANES can provide information on the contents and chemical environment of trace elements in biological samples. In the x-ray fluorescence station of BSRF, the detection limit for Fe is about 10^{-15} g [21]. With high sensitivity, collimation, and good spatial resolution (~10 μm), SRXRF analysis could provide micro-distribution map of iron in the brain regions.

Neuronal uptake and translocation of nanoscaled solid particle via neuronal axons has been described for more than 60 years [22–24]. However, it has received little attention from toxicologists. Until recently, Oberdörster et al. [11] reported that inhaled ultrafine particle ^{13}C (36 nm) could transport along axons of the olfactory nerve into the brain, which caused more attention about fine and ultrafine particle impact on CNS. In our experiment, the Fe level in the OB and brain stem slices were found to increase after 2 weeks after a single intranasal instillation of fine Fe_2O_3 particle, which suggested that iron particle entered CNS. The higher Fe levels in the ON and Gl layers indicated that Fe_2O_3 particle entered the OB via ON and could transport along the secondary nerve of Gl, where olfactory sensory neurons make contact with OB neurons and contain projections from interneurons. The increased Fe in AOE and lo indicated that Fe was transported to AOE along the axons from the mitral and tufted cells in Gl via lo. Such a conclusion is consistent with the results of inhaled ultrafine carbon particles [11] and manganese oxide particle [24]. Oberdörster et al. [11] found significant and consistent increases of ^{13}C in the OB throughout the 7-day postexposure period after the 6-h inhalation exposure to the ultrafine elemental ^{13}C particles. Fechter et al. [25] demonstrated that small particle MnO_2 (1.3 μm)

resulted in an elevation of OB manganese concentration. Lee et al. [26] found the bovine herpesvirus type 5 occurred in the areas of MOB and AO after intranasal inoculation.

The higher Fe levels in the reticular formation and spinal trigeminal regions of the brain stem indicated that iron was transported to deeper brain compartments like soluble Mn via trigeminus [27] after nasal instillation. The increase of iron levels in the brain stem has been demonstrated to be closely related with various neurodegenerative diseases, such as PD and AD [13, 15]. The reticular formation is the central core of brain stem, connecting with all parts of the brain and brain stem, and is critical for the maintenance of consciousness [28]. The increased iron level in the reticular formation indicated that Fe entered the parenchyma portion of the brain stem. Trigeminal nerve is composed of three large branches including ophthalmic (V_1, sensory), maxillary (V_2, sensory), and mandibular (V_3, motor and sensory) branches, and the major sensory innervation to the nasal cavity is supplied by sensory nerve endings of V_1 and V_2 branches of the trigeminal nerve [24]. Some of the trigeminal sensory nerve endings in the nasal epithelium also have branches directly reaching the OB [29]. Trigeminal nerve root connects the brain stem, and trigeminal nerve nucleus extends through the whole brain stem, midbrain, and medulla. Thus, based on the results of the increased Fe in the trigeminus region of brain stem, we suspect that the increased Fe in the brain stem was possibly transported via sensory nerve endings of trigeminus. Such a delivery route by trigeminal uptake of inhaled metals to enter the CNS has already been demonstrated by the study of inhaled manganese chloride in rats and mice [30]. However, the reasons for the disturbance of Fe distribution in the brain stem are unknown and need further investigation.

The mechanism of iron transport across blood–brain barrier has not yet been completely clarified. The popular accepted suggestion is that the transferrin–transferrin receptor (Tf–TfR) is the major route for iron transport across the luminal membrane of the capillary endothelium [31]. The iron possibly crosses the luminal membrane and enters the interstitial fluid in the form of Fe^{2+} [31]. The Tf–Fe and non-Tf-bound iron will be rapidly transported in the rat brain for several hours after administration of soluble iron ions [32]. But in this study, the elevated Fe content in the OB was observed even on the postexposure day 14 after a single dose of Fe_2O_3 particle intranasal instillation. Therefore, as the results, the Fe_2O_3 particle was suggested transport via olfactory pathway. Nevertheless, this result is different from the observation of Rao et al. [17], who demonstrated that $FeSO_4$ aerosol (2.99 μm) could not enter the brain via olfactory pathway. The different results might be because of the different size and chemical composition of the two kinds of iron particles. The size of the $FeSO_4$ aerosol in Rao's study was ten times of Fe_2O_3 particle used in this study; thus, the size difference might contribute to the different results. Fechter et al. [25] demonstrated that small particle aerosol deposited in the head airways taken up by olfactory nerve and transported to the OB was much more efficient than large ones.

The final chemical speciation of iron after iron particle deposition in CNS may highly associate with iron physiological function and potential neurotoxicity. The questions whether the iron particles maintain their particulate state in the deposition site or to be dissolved before translocation, during translocation, or after deposition in the destination need further study. XANES is based on the sensitivities of x-ray absorption to the valence state and neighboring atoms, which can give both structural and electronic configuration information [33]. The absorption edge energy (E_0) depends on the valence of absorption atom and could slightly shift caused by the variation of the effective atomic charge [34]. As iron in the brain is a mixture of Fe (II) and Fe (III), FeO and Fe_2O_3 were used to represent the two major valent states of iron. Such an assumption might be too simple to represent the complex speciation of iron in the brain. However, this assumption may be justified if the

chemical state of the deposited Fe_2O_3 particle was only concerned about. The Fe K-edge XANES measurement showed that the E_0 values in the OB and brain stem of the exposed mice shift to the values of Fe_2O_3. Furthermore, the elevated ratios of Fe (II)/Fe (III) in the exposed mice demonstrated that Fe (III) increased in the OB and brain stem.

Our recent results show that the Fe level in the hippocampus has increased on day 14 after intranasal exposure (data not shown here). This is in accordance with the histopathological observation at the same time point. The results demonstrated that the oxidative damage might occur in hippocampus.

In conclusion, the results demonstrated that the transportation route of inhaled Fe_2O_3 particle into the brain may be via the olfactory route or trigeminal pathway. The XANES measurement indicated that Fe (III) level in the OB and brain stem of the iron-exposed mice significantly increased compared to the controls. An important finding is that the neuron fatty degeneration in CA3 area of the hippocampus occurred in the 14th day after intranasal instillation of fine Fe_2O_3 particles.

Although there are enormous differences in nasal mucosa between rodent animals and human beings, the results may call attention to the workers at occupational potential risk for exposure to the fine iron solid particle.

Acknowledgments The authors are grateful to the foundation of National Basic Research Program of China (2006CB705605), the Chinese Academy of Sciences, and the National Natural Science Foundation of China (10490180, 20475055, 10675139).

References

1. Samet JM, Dominici FR, Curriero FCD, Coursac I, Zeger SL (2000) Fine particulate air pollution and mortality in 20 U.S. cities, 1987–1994. New Engl J Med 343:1742–1749
2. Katsouyanni K, Touloumi G, Spix C, Schwartz J, Balducci F, Medina S, Rossi G, Wojtyniak B, Sunyer J, Bacharova L, Schouten JP, Ponka A, Anderson HR (1997) Short-term effects of ambient sulphur dioxide and particulate matter on mortality in 12 European cities: results from the APHEA Project. Br Med J 314:1658–1663
3. Pope CA, Schwartz J, Ransom MR (1992) Daily mortality and PM_{10} pollution in Utah Valley. Arch Environ Health 47:211–217
4. Utell MJ, Frampton MW (2000) Acute health effects of ambient air pollution: the ultrafine particle hypothesis. J Aerosol Med 13:355–359
5. Peters A, Wichmann HE, Tuch T, Heinrich J, Heyder J (1997) Respiratory effects are associated with the number of ultrafine particles. Am J Respir Crit Care Med 155:1376–1383
6. Kreyling WG, Semmler M, Erbe F, Mayer P, Takenaka S, Schulz H, Oberdörster G, Ziesenis A (2002) Translocation of ultrafine insoluble iridium particles from lung epithelium to extrapulmonary organs is size dependent but very low. J Toxicol Environ Health 65(20):1513–1530
7. Kreyling WG, Semmler-Behnke M, Moller W (2006) Ultrafine particle lung interactions: does size matter? J Aerosol Med 19:74–83
8. Sunderman EW Jr (2001) Nasal toxicity, carcinogenicity, and olfactory uptake of metals. Ann Clin Lab Sci 31:3–22
9. Henriksson J, Tallkvist J, Tjälve H (1997) Uptake of nickel into the brain via olfactory neurons in rats. Toxicol Lett 91:153–162
10. Burd GD (1993) Morphologic study of the effects of intranasal zinc sulfate irrigation on the mouse olfactory epithelium and olfactory bulb. Microsc Res Tech 24:195–213
11. Oberdörster G, Sharp Z, Atudorei V, Elder A, Gelein R, Kreyling W, Cox C (2004) Translocation of inhaled ultrafine particles to the brain. Inhal Toxicol 16:437–445
12. DeLorenzo A (1970) The olfactory neuron and the blood–brain barrier. In: DeLorenzo A, Wolstenholme G, Knight J (eds) Taste and smell in vertebrates. CIBA Foundation Symposium Series. Churchill, London, pp 151–176
13. Korczynski RE (2000) Occupational health concerns in the welding industry. Appl Occup Environ Hyg 15:936–945

14. Thompson KJ, Shoham S, Connor JR (2001) Iron and neurodegenerative disorders. Brain Res Bull 55:155–164
15. Götz ME, Double K, Gerlach M, Youdim MBH, Riederer P (2004) The relevance of iron in the pathogenesis of Parkinson's disease. Ann N Y Acad Sci 1012:193–208
16. Elder A, Gelein R, Silva V, Feikert T, Opanashuk L, Carter J, Potter R, Maynard A, Ito Y, Finkelstein J, Oberdörster G (2006) Translocation of inhaled ultrafine manganese oxide particles to the central nervous system. Environ Health Perspect 114:1172–1178
17. Rao DB, Wong BA, McManus BE, McElveen AM, James AR, Dorman DC (2003) Inhaled iron, unlike manganese, is not transported to the rat brain via the olfactory pathway. Toxicol Appl Pharmacol 193:116–126
18. Garcia-Verdugo JM, Llahi S, Farinas I, Martin V (1986) Laminar organization of the main olfactory bulb of *Podarcis hispanica*: an electron microscopic and Golgi study. J Hirnforsch 27:87–100
19. Holstege G, Kuypers HGJM, Dekker JJ (1977) The organization of the bulbar fiber connections to the trigeminal, facial and hypoglossal motor nuclei. II. An autoradiographic tracing study in the cat. Brain 100:265–286
20. Molavi DW (1997) Neuroscience tutorial, The Washington University School of Medicine Neuroscience Tutorial. Available from: http://thalamus.wustl.edu/course/
21. Huang YY, Li GC, He W, Wu YR (1997) The progress of Beijing Synchrotron Radiation X-ray fluorescence microprobe analysis. Final Report of Institute of High Energy Physics, pp 317–319
22. Bodian D, Howe HA (1941) The rate of progression of poliomyelitis virus in nerves. Bull Johns Hopkins Hosp 69:79–85
23. Hunter DD, Dey RD (1998) Identification and neuropeptide content of trigeminal neurons innervating the rat nasal epithelium. Neuroscience 83:591–599
24. Hunter DD, Undem BJ (1999) Identification of substance P content of vagal afferent neurons innervating the epithelium of the guinea pig trachea. Am J Respir Crit Care Med 159:1943–1948
25. Fechter LD, Johnson DL, Lynch RA (2002) The relationship of particle size to olfactory nerve uptake of non-soluble form of manganese into brain. Neurotoxicology 23:177–183
26. Lee BJ, Weiss ML, Mosier D, Chowdhury SI (1999) Spread of bovine herpesvirus type 5 (BHV-5) in the rabbit brain after intranasal inoculation. J Neurovirology 5:474–484
27. Gianutsos G, Morrow GR, Morris JB (1997) Accumulation of manganese in rat brain following intranasal administration. Fundam Appl Toxicol 37:102–105
28. Parvizi J, Damasio A (2001) Consciousness and the brainstem. Cognition 79:135–160
29. Schaefer ML, Bottger B, Silver WL, Finger TE (2002) Trigeminal collaterals in the nasal epithelium and olfactory bulb: a potential route for direct modulation of olfactory information by trigeminal stimuli. J Comp Neurol 444:221–226
30. Lewis J, Bench G, Myers O, Tinner B, Staines W, Barr E, Divine KK, Barrington W, Karlsson J (2005) Trigeminal uptake and clearance of inhaled manganese chloride in rats and mice. Neurotoxicology 26:113–123
31. Malecki EA, Devenyi AG, Beard JL, Cornor JR (1999) Existing and emerging mechanisms for transport of iron and manganese to the brain. J Neurosci Res 56:113–122
32. Moos T, Morgan EH (1998) Kinetics and distribution of [^{59}Fe-^{125}I]transferrin injected into the ventricular system of the rat. Brain Res 790:115–128
33. Longa SD, Pin S, Cortès R, Soldatov AV, Alpert B (1998) Fe-heme conformations in ferric myoglobin. Biophys J 75:3154–3162
34. Yoshida S, Ektessabi A, Fujisawa S (2001) XANES spectroscopy of a single neuron from a patient with Parkinson's disease. J Synchrotron Radiat 8:998–1000